TSS-1R: SUPRATHERMAL ELECTRON DISTRIBUTIONS OBSERVED IN LOW VOLTAGE SATELLITE CONFIGURATIONS

C. Gurgiolo[1], J. D. Winningham[2], K. Wright[3] N. Stone[4]

1 Bitterroot Basic Research Inc. Hamilton, MT

2 Southwest Research Institute, San Antonio, TX

3 CSPAR, University of Alabama, Huntsville, AL

4 Marshall Space Flight Center, Huntsville, AL

Abstract. A major goal of the TSS-1R mission was to study the potential and current collection properties of a charged satellite. Data taken during the 5 hours of deployment is sufficient to begin this research, but insufficient to allow for many hard conclusions. This paper reports on the angular characteristics of both the accelerated ionospheric and the suprathermal electron distributions around the satellite in low voltage configurations (< 10V). The ionospheric electrons exhibit angular variations which appear ordered in satellite azimuth, while the angular variations observed in the suprathermal distribution appears to be ordered by the local magnetic field direction. The possible existence of a foreshock-like region upstream of the satellite will be discussed.

1. Introduction

One of the prime objectives of TSS-1R was to study satellite charging in a controlled environment. In a 5 hour deployment the satellite was released to 19.7 km where the mission prematurely ended when the tether broke. While sufficient data were obtained in

this time period to begin many of the investigations involved in the charging process, there is insufficient statistics to make many of the hard conclusions that should have resulted from the mission, and often only a hint of what is happening can often be gleaned from the data.

One of the more interesting situations arises with the satellite potential under 10V. As the satellite charges through 5V, there is a transition point, where the rammed in atomic oxygen undergoes full reflection from the satellite sheath. At this point the characteristics of the particle distributions undergo dramatic and unexpected changes (Winningham et al., 1997) as do the system IV characteristics.

In low voltage situations the dominant electron population is expected to be the accelerated ionosphere and this is true below 5V. In climbing through 5V, however, a highly directional, suprathermal electron distribution in the 90 eV to 250 eV develops and quickly becomes the dominant distribution. The transition appears related to the reflection of the incident rammed in O^+ (Wright et al., 1997).

In this paper we will look at the angular characteristics of both the accelerated ionospheric and the suprathermal electrons in low voltage situations. The implications of the development of a fore-shock like region upstream of the satellite will be discussed.

2. Instrumentation

This paper relies heavily on data taken from the Research on Orbital Plasma Electrodynamics (ROPE) experiment. The experiment has been fully described in Stone et al. [1994]. For the purpose of this paper only a brief summary is given.

ROPE consists of two banks of sensors: three azimuthally co-aligned soft particle

spectrometers (SPES) flush mounted on the satellite and two SPES and a differential ion flux probe (DIFP) mounted on the end of a fixed boom, one satellite radius from the surface. The boom sensors can be independently biased to the local floating potential.

The two boom mounted SPES are equatorial mounted, looking radially toward and away from the satellite (sensors 1 and 2 respectively). The surface mounted SPES are located 135° antispinward from the fixed boom, and at elevations of 7° (sensor 3), 45° (sensor 4), and 85° (sensor 5). The three equatorial sensors have both electron and ion channels while the two out of plane sensors measure electrons only.

All sensors complete a full energy sweep in 2.048 second giving roughly a 3° azimuthal resolution. The equatorial sensors have roughly the same sensitivity while the off equatorial sensors are less sensitive by a factor of $\approx 10^4$.

3. Data

An overview of two of the three time periods analyzed in this paper is shown in Figure 1. The three panels contain electron data presented in energy-time spectrogram format for the satellite mounted sensors, beginning with sensor 3. Note the difference in ranges between the colorbars for sensor 3 and sensors 4 and 5, reflecting the different sensitivities.

The two low voltage events occur between 23:44:45 - 23:46:45 UT (Event 1) and 23:51:45 - 23:55:30 UT (Event 2). The events bracket a high-voltage event not to be discussed here. Being separated by only 5 minutes, the two events occur under near identical conditions. During Event 1 the satellite floated slightly above the 5 V transition voltage, at 8 - 9 V and the average tether current was steady at 52 ma. In Event

2 the satellite voltage sat just below the transition voltage at 3 - 4.5 V with a slightly higher average tether current of 57 ma.

For so little difference in current there is a marked difference in the electron flux observed at the satellite. This apparently results from instabilities associated with the reflection of the rammed O^+ (Papadopolous et al., 1997).

The satellite charge is reflected in the thin band of intense electrons seen in sensor 3. These are the ionospheric electrons which have fallen through the satellite sheath. While a similar signature should be present in sensors 4 and 5, it is not, for two reasons: 1) the charging flux is often too small to warrant a response in these sensors; and 2) when a response might be expected, the charging flux generally buried beneath the background flux in these sensors.

In addition to the charging signature, both events exhibit a suprathermal electron signature in the 90 to 200 eV range. This population appears unique to the TSS-1R charged satellite and the conditions under which the measurements occurred, in particular the high relative velocity of the satellite with respect to the local plasma.

Contrasting the two events, it is evident that as the satellite voltage climbs through 5V the suprathermals rise in intensity and spread both in azimuth and in elevation. For satellite potentials above 5V they are the dominant plasma population. Note that even with the satellite siting at or near 0V, however, there is a weak suprathermal signature (see the beginning of Figure 1 and the time between Event 1 and the high voltage event).

The suprathermals are highly collimated in polar angle and do not extend much below 20° - 30degrees. That they are seen at all in sensor 3 is due to its large geometry factor. Remember that sensor 3 is 10^4 times more sensitive than either sensors 4 or 5, yet in both

events it is well away from saturation.

Both the accelerated ionosphere and the suprathermal electrons form well defined peaks in velocity space and are reasonably fit by a Maxwellian distribution of the form:

$$f = N\left(\frac{m}{2\pi kT}\right)^{-\frac{3}{2}} e^{\frac{-m(v-V)^2 + e\phi}{2T}}$$

with V set to 0 when fitting the charging peak and ϕ set to zero when fitting the suprathermal peak. The fits allow estimates to be made of the density, energy and temperature of both populations.

The density and energy estimations derived from Event 2 are shown in Figure 2. The figure consists of four sets of concentric rings, each comprised of two separate bands. Running from inner-most to outer-most, the rings show the estimated density (inner band) and average energy (outer band) for the accelerated ionospheric electrons and the suprathermal electrons as seen in sensors 3, 4, and 5 respectively. The average energy of the ionospheric electrons is equivalent to the satellite potential.

Colors are translated to values using the colorbars on the right. Dual ranges are given for the suprathermal density with the inner scale to be used for sensor 3 and the outer for sensors 4 and 5.

The average equatorial projection of B is indicated by the vector in the inner circle. The solid line points to the beginning of the event with the attached arc showing both the angular extent of the event as well as the satellite rotation direction.

Small gaps in the data are areas where the peak was not sufficiently formed for a successful fit. Larger gaps, however, indicate that the peaks were not present in the data.

The large gap in the ionospheric component is the local electron wake.

Figure 3 has an identical format to Figure 2 but combines data from two events, which although separated in time, occurred under identical satellite configuration. Most of the external variables are the same within acceptable tolerances. Ancillary data for each event is distinguished by color (white or cyan).

The major differences between the two events occur in the voltage across the circuit, about 2 keV for earlier event and close to 3.5 keV for later event, and in the average tether current which was 122 ma in later event, almost 2.5 times larger then the earlier.

4. Discussion

The ionospheric electrons show ordering with satellite azimuth which is reasonably symmetric about the local electron wake. This straddles the satellite wake in Figure 3, and in Figure 2 it is skewed to the right. In both figures the density peaks slightly to the left of satellite ram, but in general, smoothly decreases towards the electron wake as the satellite shielding becomes more and more effective.

In both events, the ionospheric data point to a differentially charged satellite. There is a distinct minimum in the potential opposite the electron wake with the potential building symmetrically along either side, reaching a maximum just before the sensors enter the wake. This was not expected in TSS and may be due to emission from the satellite skin in response to nonuniform incident local electron fluxes.

The suprathermal electrons are much more complex in their overall structure, especially as the satellite climbs above 5V and they intensify to become the dominant population. In every case looked at, the suprathermals appear confined to the upper

portion of the satellite top hemisphere. (Recall there is no data from the lower hemisphere). In Figure 3 the density peaks in azimuth about −45degrees in sensor 4. This brackets 0° pitch-angle.

Both Figures 2 and 3 show a distinct left-right asymmetry in the data. To the right of ram the suprathermals are more intense and dynamic. This is reminiscent of the magnetic ordering which is observed upstream of the Earth's bow shock where the tangent line of the interplanetary field with the bow shock divides the upstream into an active, magnetically attached foreshock region and a quiescent detached region. From the local magnetic field orientation, the equivalent to the foreshock would lie to the right in both figures. In a foreshock-like picture, the suprathermal electrons would be the by-product of instabilities generated in the upstream region resulting from the ion reflection at the sheath which are then convected back into the satellite. The scale size of the satellite in relation to the particle gyroradii would preclude observations of sharp foreshock cut-off as observed upstream of the bow shock, still the overall asymmetry would be seen.

With an active foreshock it might be expected that the measured maximum in the estimated ionospheric density would fall to the left of ram. Scattering by turbulence in foreshock could reduce the estimated density observed when the sensors are on the foreshock side of the satellite.

In addition to the left-right asymmetry, in the suprathermals there are two other features worthy of note. The first is the anisotropy in the estimated peak energy for each of the 3 satellite mounted sensors. The energy maximizes in both the extreme sensors, being a minimum in sensor 4. In addition the energy peaks in the satellite wake for both sensors 3 and 5.

5. Conclusions

Particle observations at the TSS-1R satellite in low voltage situations indicate the following:

1. A near step-like jump in the particle flux to the satellite as the potential passes through 5V.
2. A switch in the dominant plamsa from the ionospheric component to the suprathermal component as the potential passes through 5V.
3. The ionospheric data is reasonably ordered in azimuth about the local electron wake.
4. The satellite is differential charged.
5. The suprathermals are spatially non-isotropic confined above $\approx 20°$ to $30°$ in elevation with a maximum consistent with a field aligned beam.
6. The data supports the idea of a foreshock like region upstream of the satellite.

Acknowledgements. Two of us, CG and JDW, would like to acknowledge support by NASA Contract NAS8-36840 and one us, KW, would like to acknowledge support by NASA Contract NAS8-37107.

References

Stone, N. H., et al., A technical description of the TSS-1 ROPE investigation, *Il Nuovo*

Cimento, 17C, 85, 1994.

Papadopolous, K., Chang., C. L., and Drobot, A. Ion reflection in TSS-1R, *Geophys. Res. Lett., this issue*, 1997.

Winningham, J. D., et al., Suprathermal electrons observed on the TSS1-R satellite, *Geophys. Res. Lett., this issue*, 1997.

Wright, K. H., et al., Observations of reflected ions and plasma turbulence for satellite potentials greater than the ion ram energy, *Geophys. Res. Lett., this issue*, 1997.

Figure Captions

1 Overview of the two low voltage events. The first event occurs between 23:44:45 and 23:46:45 UT and the second between 23:51:45 and 23:55:30 UT.

2 Azimuthal and polar overview of the sub-5V charging event

3 Combined azimuthal and polar overviews of two events with the >5V satellite charging.

1996/056/23:44:14:723

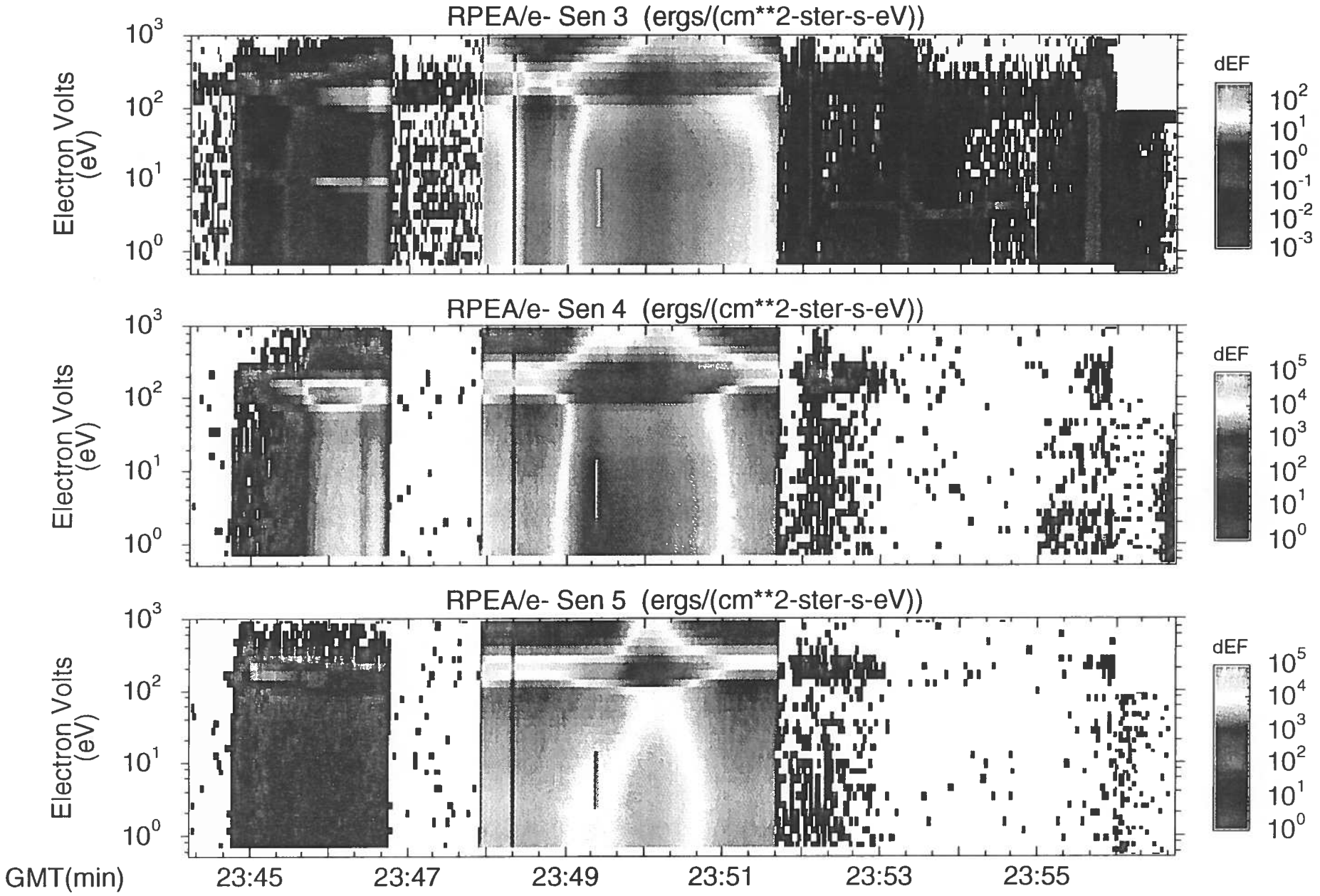

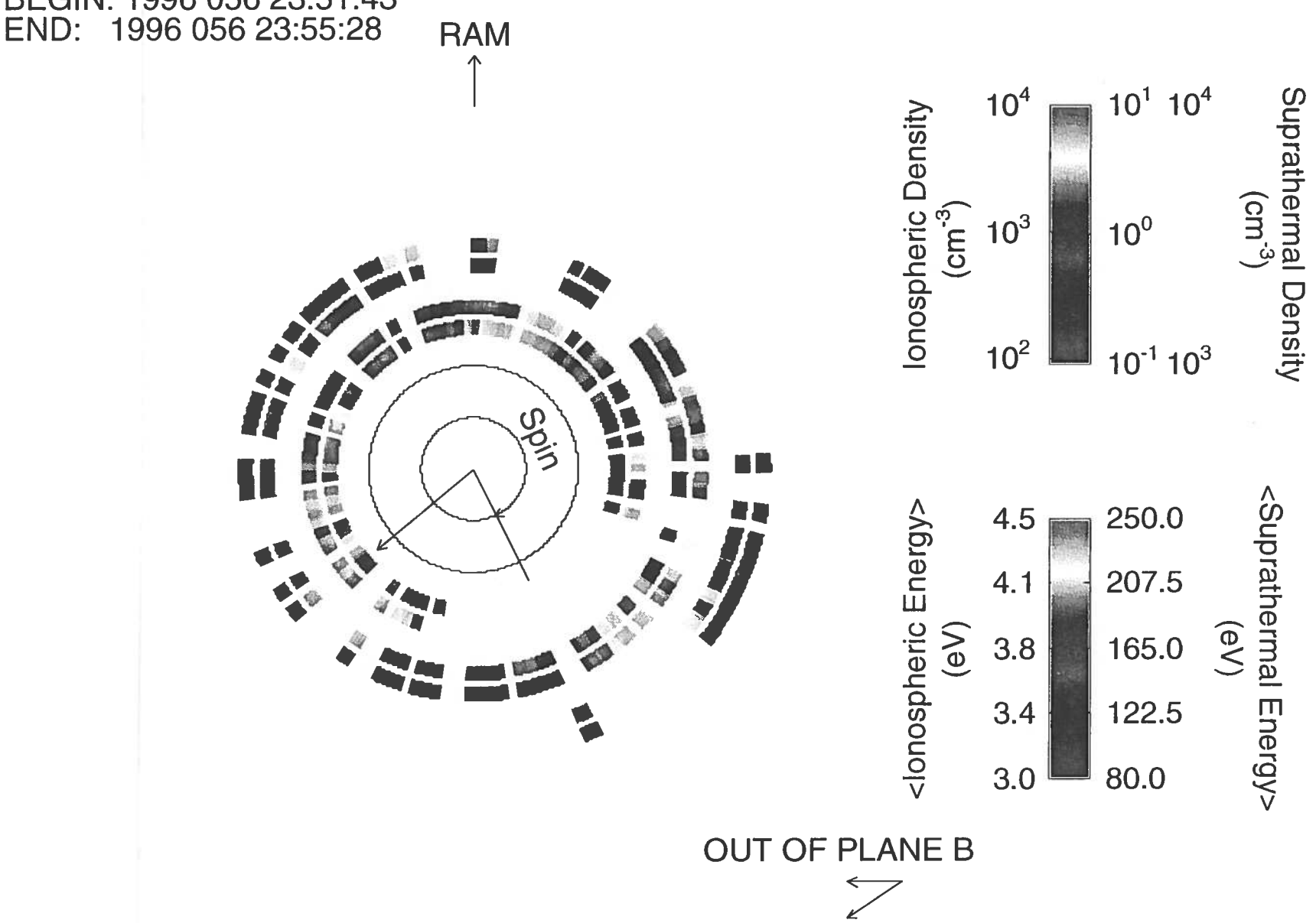
BEGIN: 1996 056 23:51:43
END: 1996 056 23:55:28
RAM
Spin
Ionospheric Density (cm-3)
10^4
10^3
10^2
10^1 10^4
10^0
10^-1 10^3
Suprathermal Density (cm-3)
<Ionospheric Energy> (eV)
4.5
4.1
3.8
3.4
3.0
250.0
207.5
165.0
122.5
80.0
<Suprathermal Energy> (eV)
OUT OF PLANE B

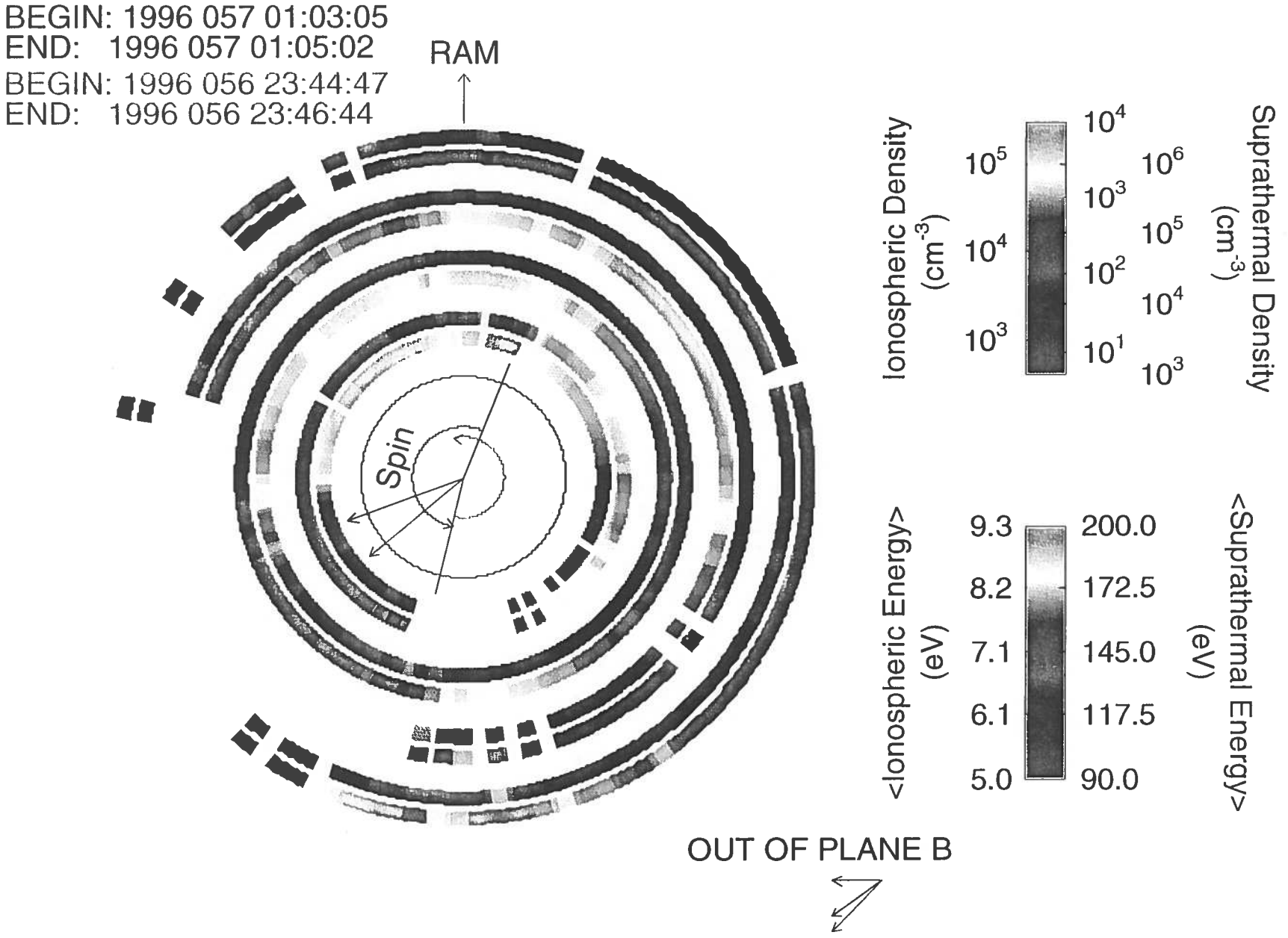
BEGIN: 1996 057 01:03:05
END: 1996 057 01:05:02
BEGIN: 1996 056 23:44:47
END: 1996 056 23:46:44
RAM
Spin
Ionospheric Density (cm-3)
10^5
10^4
10^3
10^4
10^3
10^2
10^1
10^6
10^5
10^4
10^3
Suprathermal Density (cm-3)
<Ionospheric Energy> (eV)
9.3
8.2
7.1
6.1
5.0
200.0
172.5
145.0
117.5
90.0
<Suprathermal Energy> (eV)
OUT OF PLANE B

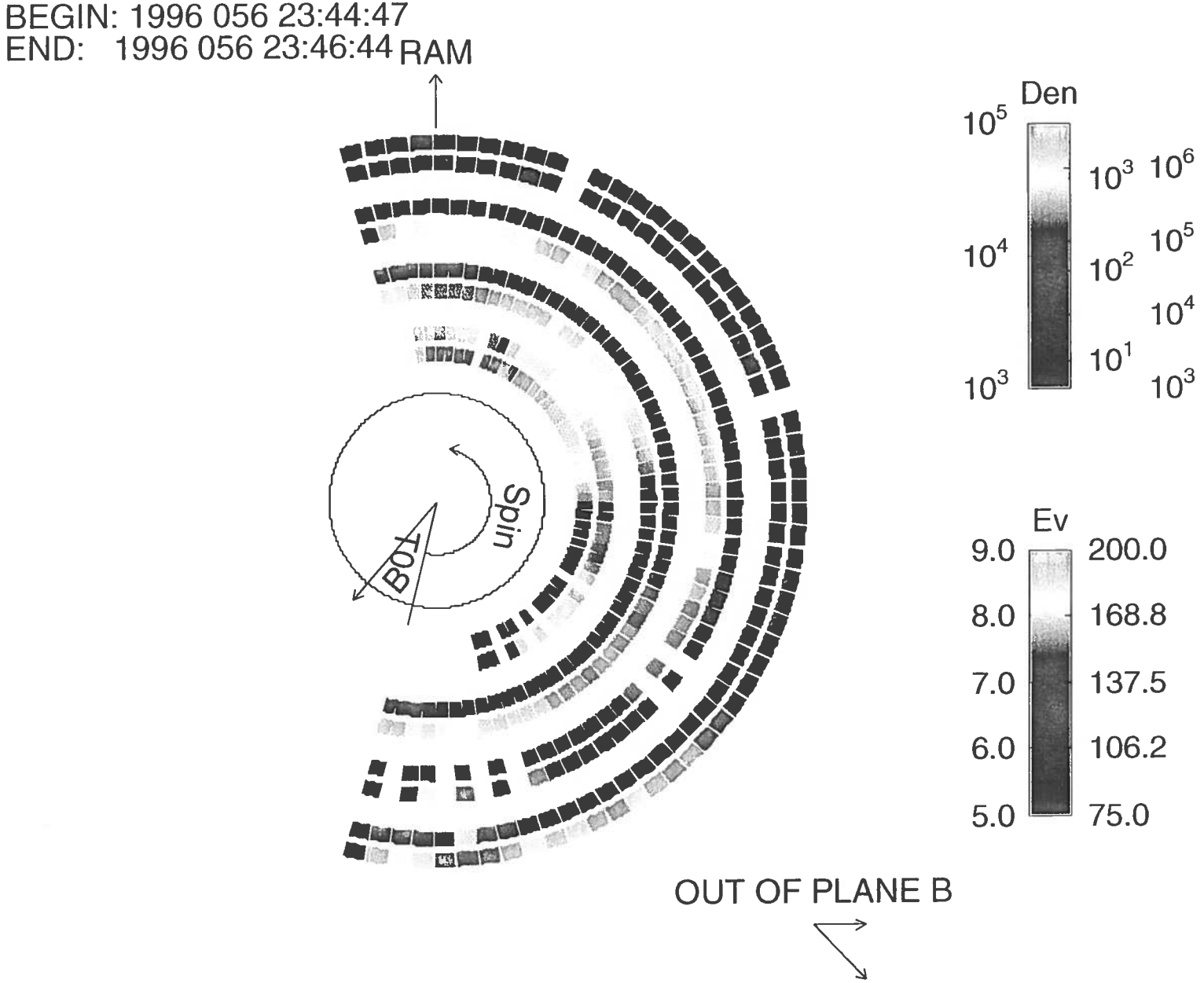
BEGIN: 1996 056 23:44:47
END: 1996 056 23:46:44
RAM
Den
10^5
10^4
10^3
10^3 10^6
10^2 10^5
10^1 10^4
10^3
Spin
BOT
Ev
9.0
8.0
7.0
6.0
5.0
200.0
168.8
137.5
106.2
75.0
OUT OF PLANE B

Figure 2.

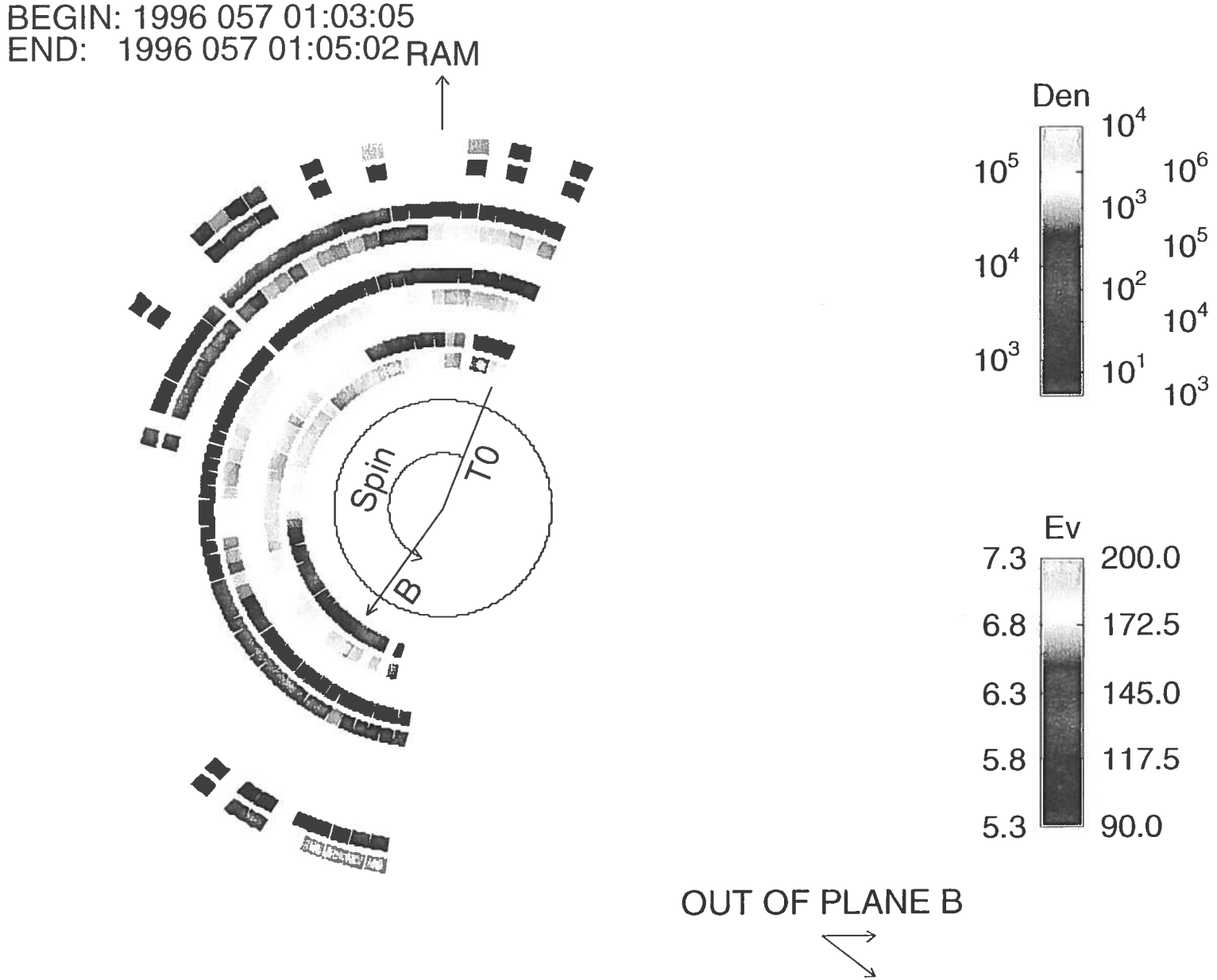
BEGIN: 1996 057 01:03:05
END: 1996 057 01:05:02
RAM
Spin
T0
B
Den
10^4
10^5
10^6
10^3
10^5
10^4
10^2
10^4
10^3
10^1
10^3
Ev
7.3
200.0
6.8
172.5
6.3
145.0
5.8
117.5
5.3
90.0
OUT OF PLANE B

Figure 3.

1996/056/23:44:14:723

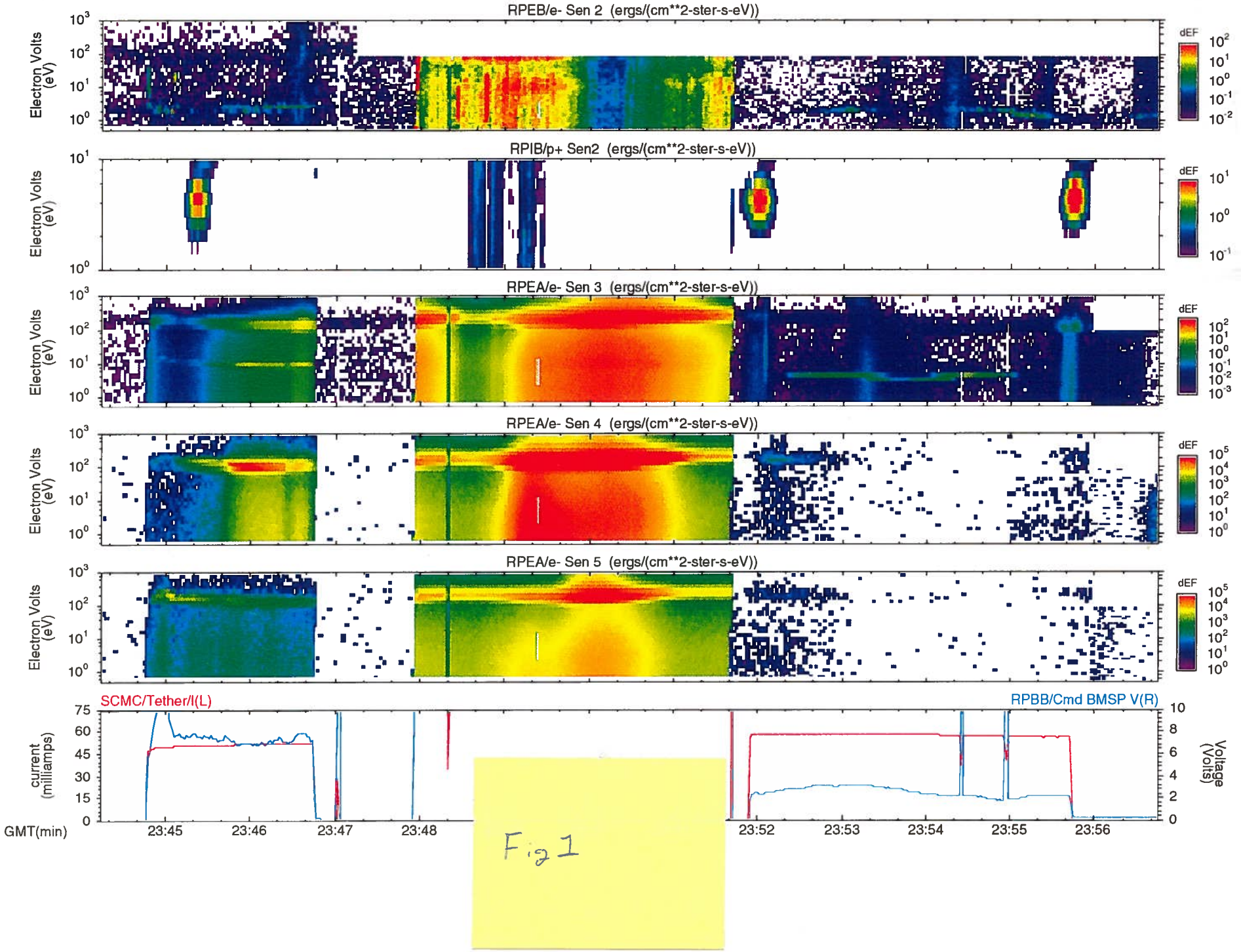

Fig 1

1996 056
23:46:31 940 to23:46:33 924

Fig 2

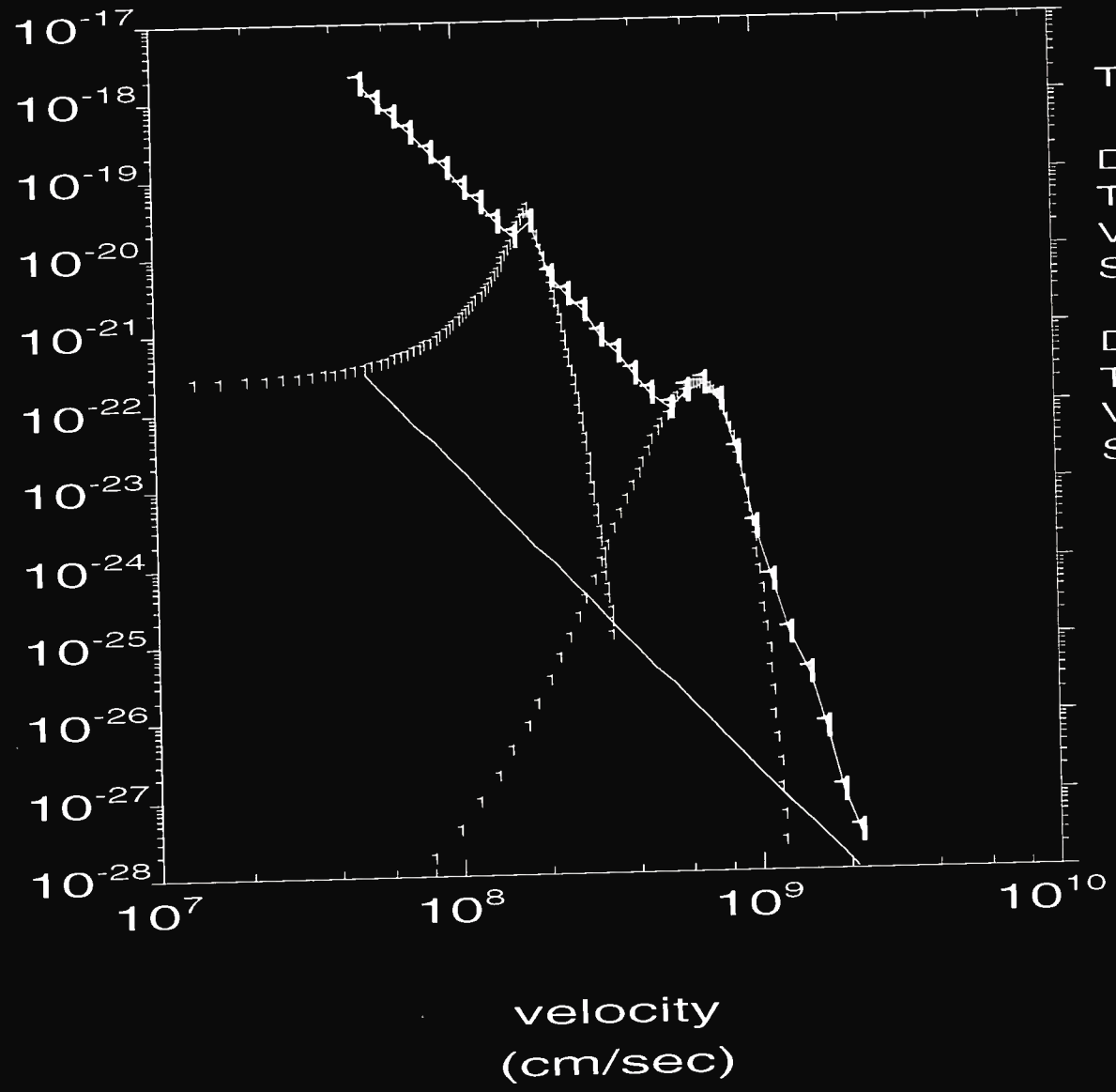

TSS/ROPE/RPEA

D = 1.0257e+05
T1 = 1.717
Vx: 1752 / E: 8.73
SD = 0.026

D = 3.8241e+03
T1 = 6.633
Vx: 6511 / E: 120.52
SD = 0.047

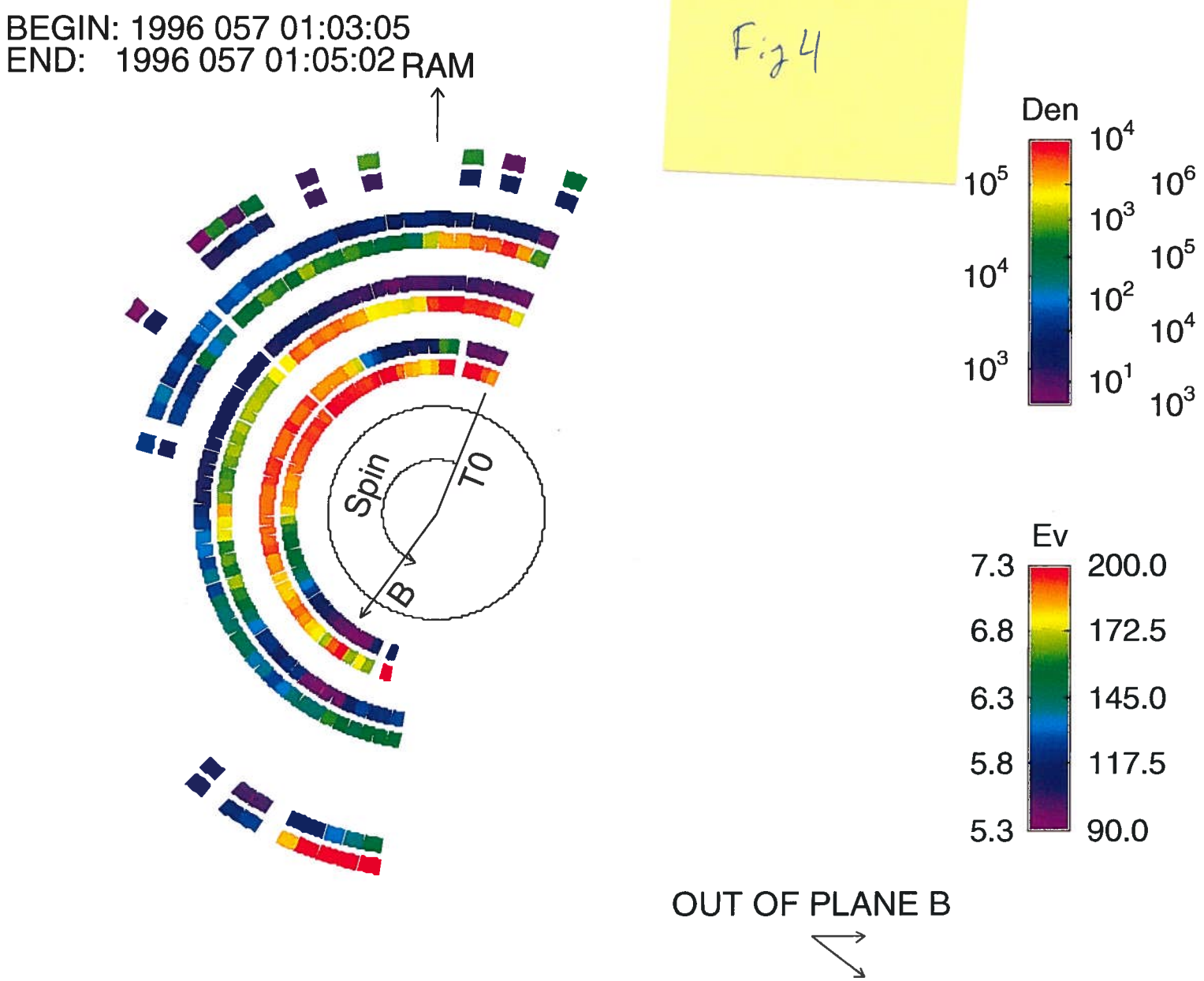
BEGIN: 1996 057 01:03:05
END: 1996 057 01:05:02
RAM
Spin
T0
B
Den
10^4
10^5
10^6
10^3
10^5
10^4
10^2
10^4
10^3
10^1
10^3
Ev
7.3
200.0
6.8
172.5
6.3
145.0
5.8
117.5
5.3
90.0
OUT OF PLANE B

Fig 4